Supporting information for

Advanced sodium-ion battery anode material prepared by regulating an environmentally friendly hard carbon precursor through bio-based molecular coupling

Kewu Zhou, Jie Li, Shaoqiu Zheng, Yu Zhang, Yue Zhou, Xinhua Yuan

(School of Materials Science and Engineering, Jiangsu University, Zhenjiang, Jiangsu, China, 212013)

(Corresponding author: Xinhua Yuan, E-mail: yuanxh@ujs.edu.cn)

S1. Experimental section

Material synthesis

Preparation of RG

Resorcinol (≥99.7%, Sinopharm Chemical Reagent Co., Ltd.), glyoxylic acid (≥98%, Shanghai Aladdin Biochemical Technology Co., Ltd.) and oxalic acid (≥99.8%, Shanghai Aladdin Biochemical Technology Co., Ltd.) were dissolved in anhydrous ethanol (≥99.7%, Sinopharm Chemical Reagent Co., Ltd.) at specific ratios (molar ratio of resorcinol to glyoxylic acid = 1:2, mass of oxalic acid = 20% of resorcinol mass). After being reacted at 95°C for 4 hours, the solution was transferred to an autoclave and subjected to hydrothermal reaction at 180°C for 12 hours to obtain the hard carbon precursor RG. Subsequently, RG was placed in a tube furnace and pyrolyzed at 1400°C for 2 hours under high-purity argon atmosphere at heating rate of 5°C/min. The resulting hard carbon material was labeled as RG-1400.

Preparation of LRG

Alkali lignin (LR, Tokyo Chemical Industry Co., Ltd.), resorcinol and oxalic acid were dissolved in anhydrous ethanol at specific ratios (mass ratio of lignin to resorcinol

= 1:5, molar ratio of resorcinol to glyoxylic acid = 1:4). The mixture was reacted at 90°C for 2 hours to form prepolymer. After natural cooling to 60°C, glyoxylic acid was added, and the temperature was raised to 95°C for further 4-hour reaction. The resulting solution was transferred to an autoclave and subjected to hydrothermal reaction at 180°C for 12 hours to obtain the hard carbon precursor LRG. Finally, LRG was placed in a tube furnace and pyrolyzed at 1400°C for 2 hours under high-purity argon atmosphere at heating rate of 5°C/min. The resulting hard carbon material was labeled as LRG-1400.

S2. GITT measurements and calculation of sodium-ion diffusion coefficients

1. Measurement conditions

GITT measurements were carried out at the fourth cycle at a current density of 20 mA g^{-1}. Each pulse step consisted of a 30-min galvanostatic discharge or charge followed by a 30-min relaxation period to allow the electrode potential to approach equilibrium. The voltage window was 0.001-2.5 V. The first three cycles were performed under the same current density as formation cycles to establish a stable SEI film.

2. Calculation formula for the sodium-ion diffusion coefficient

The sodium-ion diffusion coefficient (D_{Na^+}) was calculated according to a simplified form of Fick's second law. When the relaxation time is sufficiently long and the voltage exhibits a linear relationship with $\tau^{1/2}$, D_{Na^+} can be obtained from the following equation:

$$D_{Na^+} = \frac{4}{\pi\tau}\left(\frac{m_B V_M}{M_B S}\right)^2\left(\frac{\Delta E_s}{\Delta E_t}\right)^2$$

The parameters are defined in the table below:

Parameter	Definition	Value / Remark
τ	Pulse duration (s)	1800
m_B	Active material mass (g)	Calculated from electrode loading
V_M	Molar volume (cm^3 mol^{-1})	~7.5
M_B	Molar mass (g mol^{-1})	12.01
S	Electrode/electrolyte contact area (cm^2)	~0.785
ΔE_s	Steady-state voltage change induced by the pulse (V)	Read from the GITT curves
ΔE_t	Transient voltage change during the pulse (V)	Read from the GITT curves

S3. Mass breakdown of full-cell components and estimation of practical energy density

1. Calculation assumptions

The full cell tests were performed using CR2032 coin type cells. Both cathode and anode disks were punched to a diameter of 10 mm (area ≈ 0.785 cm^2). The mass of each component is taken as follows:

Component	Areal loading / amount per cell	Mass per cell (mg)	Data source
Cathode active material (NFM)	3.5 mg cm^{-2}	2.75	Coating loading × electrode area
Anode active material (NLRG-1400)	1.6 mg cm^{-2}	1.26	Coating loading × electrode area
Al foil current collector (cathode side)	~3.0 mg cm^{-2}	2.36	Supplier specification
Cu foil current collector (anode side)	~8.7 mg cm^{-2}	6.83	Supplier specification
Conductive additive + binder	10% of electrode mass	0.40	Estimated based on active material : carbon : binder = 80:10:10
Separator (GF/F)	—	~15.0	16 mm disk, supplier specification
Electrolyte (1.0 M $NaPF_6$ in DIGLYME)	130 μL	156.0	Density taken as 1.2 g mL^{-1}
CR2032 casing + spring + spacer	—	~2300.0	Measured average value

2. Energy density based on different mass scopes

Discharge energy of a single full cell = cathode specific capacity × cathode active material mass × average operating voltage:

Discharge energy = 125.8 mAh g^{-1} × 2.75 mg × 2.8 V = 0.969 mWh

Calculation basis	Included components	Total mass (mg)	Energy density (Wh kg^{-1})
Total active material mass	Cathode + anode active materials	4.01	241
Total electrode coating mass	+ conductive additive + binder	4.41	220
Including current collectors	+ Al foil + Cu foil	13.60	71
Including electrolyte & separator	+ separator + electrolyte	184.60	5.2

All components (including casing)	+ casing/spring/spacer	2484.60	0.39

3. Conclusion

As shown in the table above, the energy density decreases substantially as inactive components are progressively included. In particular, the mass of the stainless-steel casing, spring and spacer in a CR2032 coin cell (~2.3 g) accounts for more than 90% of the total mass, leading to a cell-level energy density of less than 1 Wh kg^{-1} when all components are counted. This value carries limited practical significance at the coin-cell research stage. Therefore, following the common practice in the academic literature, only the energy density based on the total active material mass of the anode and cathode (241 Wh kg^{-1}) is reported in the main text, which is also the widely adopted calculation method in the references cited for comparison (Table. S6).

Table. S1 Comparison of main anode material types for sodium-ion batteries.

Na-storage mechanism	Typical materials	Main advantages	Key challenges
Intercalation-type	Hard carbon, Graphite	Long cycle life, low cost, stable structure	Low ICE (hard carbon), extremely low capacity for graphite
Conversion-type	Fe_2O_3, MoS_2	High theoretical capacity	Low ICE, large voltage hysteresis, significant volume change
Alloying-type	Sn, Sb, Bi	Very high specific capacity	Huge volume expansion (>300%), poor cycling stability
Conversion-alloying	SnO_2, Sb_2S_3	Relatively high capacity	Complex mechanism, still subject to volume expansion
Na metal anode	Na foil	Highest capacity, lowest potential	Na dendrites, unstable SEI, safety hazards

Table. S2 Semi-quantitative comparison of green metrics between the bio-based route (NLRG) in this work and the conventional phenol-formaldehyde (PF) route.

Evaluation dimension	Conventional PF route	Bio-based NLRG route (this work)	Comparative remark
Feedstock toxicity / Renewable carbon content	Phenol (highly toxic), formaldehyde (carcinogenic/teratogenic); renewable carbon content ~0%	Naringenin (natural polyphenol), lignin (biopolymer), glyoxylic acid (green aldehyde source); renewable carbon content >80%	Hazardous monomers are eliminated at the source, in alignment with the green chemistry principles of "use of renewable feedstocks" and "reduction of hazardous substances"
Carbon residue rate	~41.8% (literature value [42])	~46.1% (TGA measurement, this work)	A higher carbon residue rate is exhibited by the NLRG route, requiring less precursor to produce 1 kg of hard carbon (2.17 kg vs. 2.39 kg)
Solvent recovery rate	Ethanol/water system, recovery rate ~85%	Anhydrous ethanol system, recovery rate >85%	Comparable; ethanol can be recovered by distillation and reused in both routes
Specific energy consumption per unit product ($kWh\ kg^{-1}$ hard carbon)	~42.7	~55.8	The comprehensive energy consumption of the NLRG route is moderately higher due to the additional hydrothermal treatment step, but the gap remains within the same order of magnitude; if the energy overhead associated with emission control and occupational protection against highly toxic monomers in the PF route is taken into account, the actual energy consumption gap between the two routes would be further narrowed

Key waste streams	Wastewater containing formaldehyde and phenol, requiring rigorous detoxification	Saline wastewater (NaCl), dischargeable after neutralization	Highly toxic organic waste streams are avoided in this route, and the difficulty and cost of wastewater treatment are substantially reduced

Calculation notes:

1. Carbon residue rate: PF route ~41.8% (literature value [42]); NLRG route ~46.1% (TGA measurement, this work). Approximately 2.39 kg of precursor is required to produce 1 kg of hard carbon for the PF route, whereas only approximately 2.17 kg is required for the NLRG route.

2. Energy consumption estimation: Based on a single batch processing 50 g of precursor, including stirred reaction (~2 kWh), hydrothermal treatment (~3 kWh, NLRG route only, including heating/holding/cooling), and high-temperature pyrolysis (~15 kWh, including heating/holding/cooling/Ar). The PF route does not involve a hydrothermal step, and a comprehensive energy consumption of approximately 42.7 kWh is required to produce 1 kg of hard carbon; for the NLRG route, although a higher carbon residue rate is achieved and less precursor is required, a comprehensive energy consumption of approximately 55.8 kWh kg^{-1} is incurred due to the additional hydrothermal treatment energy. The two values remain within the same order of magnitude.

3. Solvent recovery: Both routes employ ethanol as the primary solvent, with recovery rates exceeding 85% under laboratory conditions.

4. Renewable carbon content: Refers to the molar percentage of carbon atoms derived from biomass (non-fossil) sources relative to the total carbon atoms in the feedstock. In the PF route, both phenol and formaldehyde are petrochemical-derived. In the NLRG route, naringenin, lignin, resorcinol and glyoxylic acid are all biomass-derived or green-synthesized products.

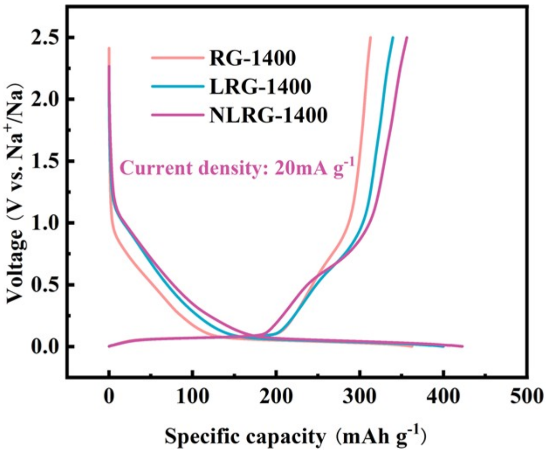

Fig. S1 Galvanostatic charge/discharge curves of RG-1400, LRG-1400, and NLRG-1400 at 20 mA g^{-1}.

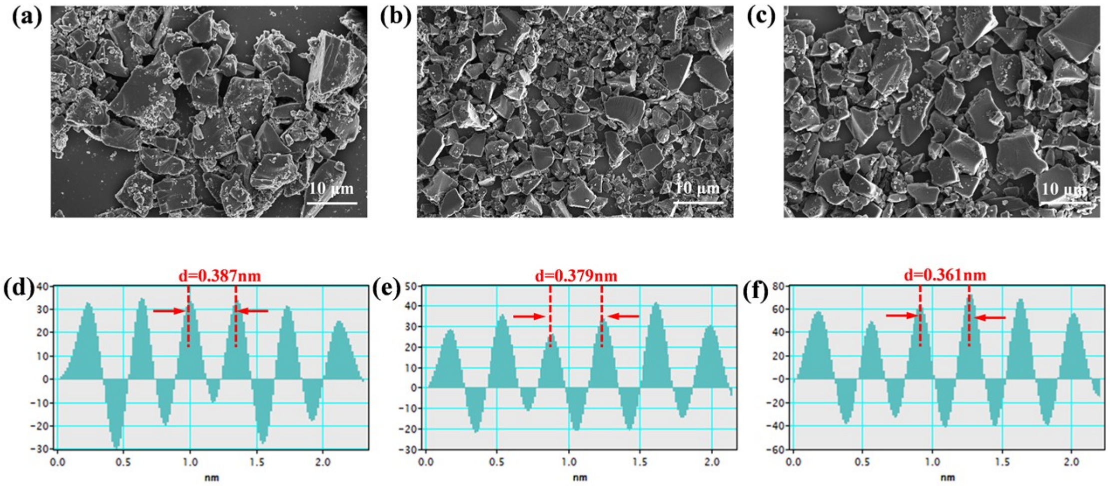

Fig. S2 SEM images and carbon interlayer spacing maps of (a,d) NLRG-1200, (b,e) NLRG-1400, and (c,f) NLRG-1600 are presented.

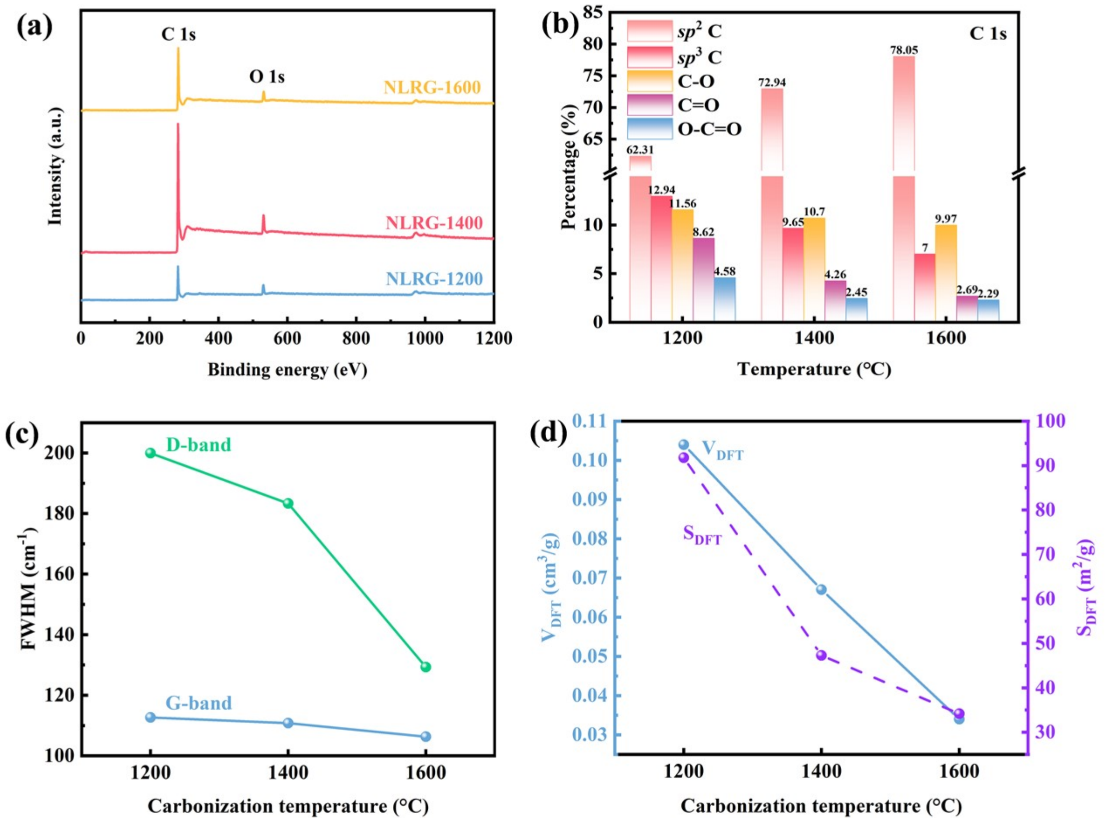

Fig. S3 (a) Full-scan XPS spectra of NLRG-1200, NLRG-1400 and NLRG-1600; (b) Area ratios of C/O bonds based on high-resolution C 1s spectral fitting; (c) Relationship between pyrolysis temperature and FWHM; (d) DFT total pore volume (V_{DFT}) and DFT total pore surface area (S_{DFT}) as a function of pyrolysis temperature.

Table. S3 The structural parameters of NLRG-1200, NLRG-1400, and NLRG-1600.

Sample	I_D/I_G	L_c (nm)	L_a (nm)	$d_{(002)}$ (nm)	D-band (cm^{-1})	G-band (cm^{-1})	A_{BET} (nm)	S_{BET} (m^2/g)	V_{DFT} (cm^3/g)	S_{DFT} (m^2/g)
NLRG-1200	1.93	2.787	5.761	0.387	199.90	112.66	2.32	173.52	0.104	91.75
NLRG-1400	1.86	3.162	6.537	0.379	183.29	110.78	2.39	113.03	0.067	47.28
NLRG-1600	1.43	3.891	8.045	0.361	129.30	106.30	3.67	35.83	0.034	34.16

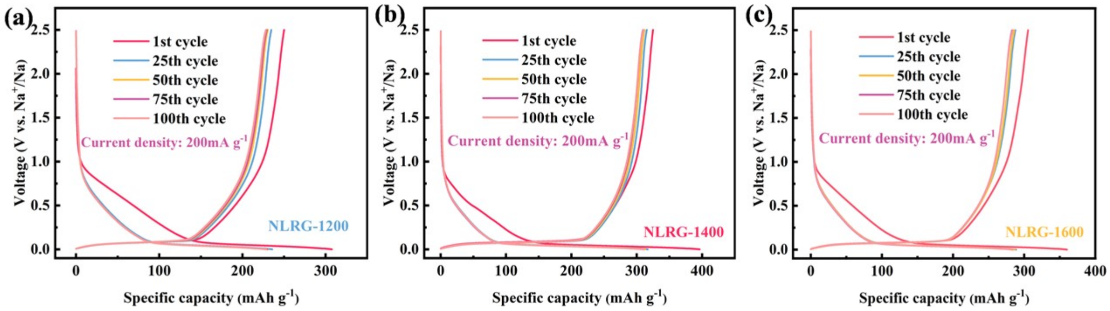

Fig. S4 (a,b,c) Galvanostatic charge/discharge curves of NLRG-1200, NLRG-1400 and NLRG-1600 at different cycle numbers, respectively.

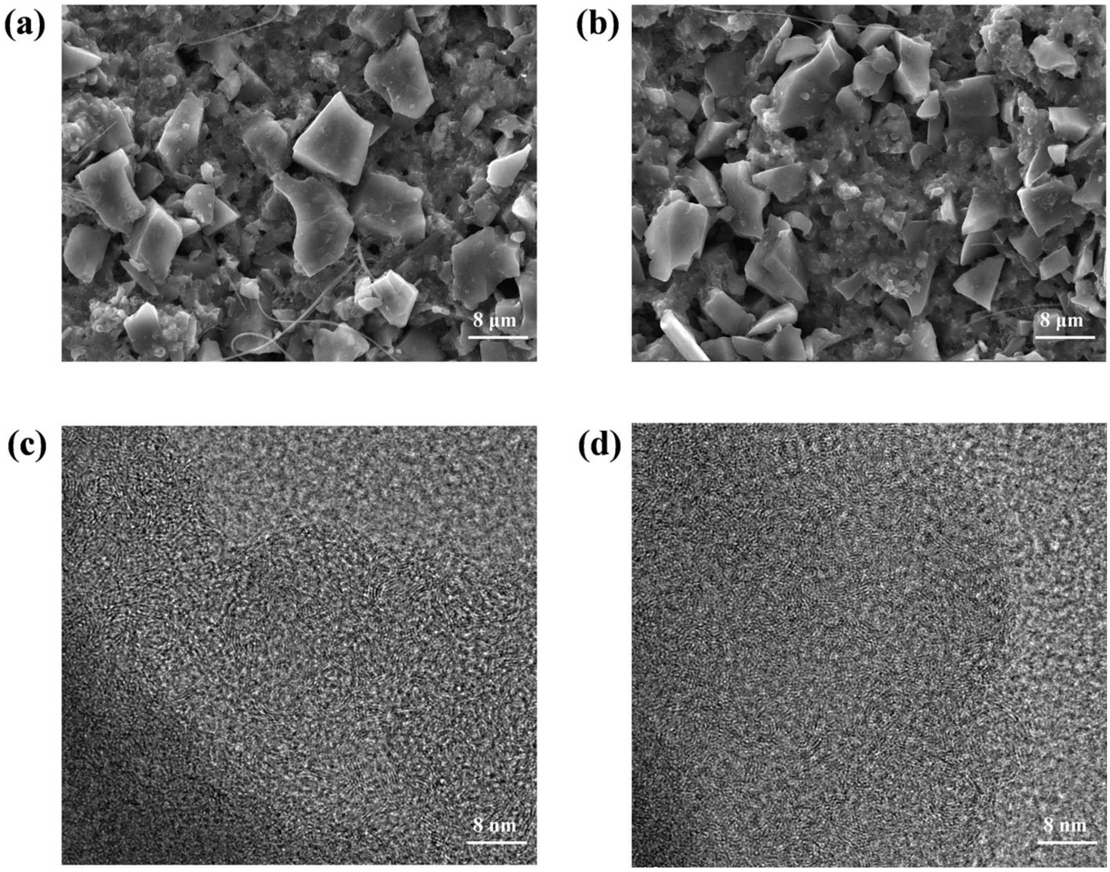

Fig. S5 Ex-situ SEM and HR-TEM images of the NLRG-1400 electrode after 100 cycles at a current density of 200 mA g^{-1}. (a, b) SEM images; (c, d) HR-TEM images.

Table. S4 The NLRG-1400 hard carbon is compared with various hard carbons reported in recent literature in terms of initial reversible capacity, ICE, cycle number, and capacity retention.

Serial Number	Reference	Initial Reversible Capacity (mAh g^{-1})	ICE (%)	Cycle Number (n)	Capacity Retention (%)
1	1	343	81	500	81
2	2	337.3	90	600	92
16	16	310	85	100	93
17	17	308	90.1	100	42
18	18	327.9	89	1000	84
20	20	133	38.1	100	88.4
21	21	323	85	50	92.3
22	22	323	86.4	—	—
24	24	284	88	—	—
25	25	338	57.3	800	55
26	26	—	—	100	91
27	27	271	69.9	150	54.2
28	28	325	88.59	300	89
29	29	334.3	82.1	—	—
30	30	334.3	84.7	300	85
31	31	351	72	—	—
32	32	361	75.9	350	85
33	33	351	83	—	—
40	40	270	71.6	—	—
43	43	390	70.9	400	80
44	44	—	—	1000	52.8
45	45	325	91.5	—	—
46	46	360.96	82	500	94
48	48	278	85	800	89
49	49	481.5	72.1	100	91.5
50	50	—	—	100	96
This work	—	**356.2**	**84.2**	**1000**	**90.5**

Table. S5 A comparison of the rate performance between NLRG-1400 hard carbon and various hard carbons reported in recent literature is performed.

Serial Number	Reference	Current density (mA g^{-1}) – Reversible capacity (mAh g^{-1})									
22	22	40-335	100-272.61	200-222.04	500-132.74	—	—	—	—	—	—
24	24	30-284	40-253.13	100-232.7	200-183	400-92.62	—	—	—	—	—
25	25	30-338	50-254.24	100-203.62	200-153.85	500-122.1	1000-101	—	—	—	—
27	27	12-271	24-228.69	60-181.41	120-161.57	240-151.29	—	—	—	—	—
28	28	20-325	40-302.36	100-281.75	200-265.3	400-233.9	1000-164.47	—	—	—	—
30	30	20-334.3	50-273	100-208	200-103	500-84	750-73	1000-63	—	—	—
31	31	50-351.1	200-205.61	500-103.5	1000-85.8	—	—	—	—	—	—
32	32	20-361	50-306.49	100-245.27	200-112.66	500-87.17	1000-63.9	—	—	—	—
47	47	100-300	200-277.6	500-227.36	1000-187.81	—	—	—	—	—	—
49	49	100-276.8	200-186.08	500-106.57	750-86.22	1000-56.6	—	—	—	—	—
50	50	20-350	50-296.72	100-266.26	200-206.61	500-105	1000-76.7	—	—	—	—
This work	—	**20-356.**	**40-338.**	**60-331.**	**80-326.**	**100-322.**	**200-310.**	**400-289.**	**600-267.**	**800-244.**	**1000-**

		17	96	84	49	61	6	03	31	74	224.43

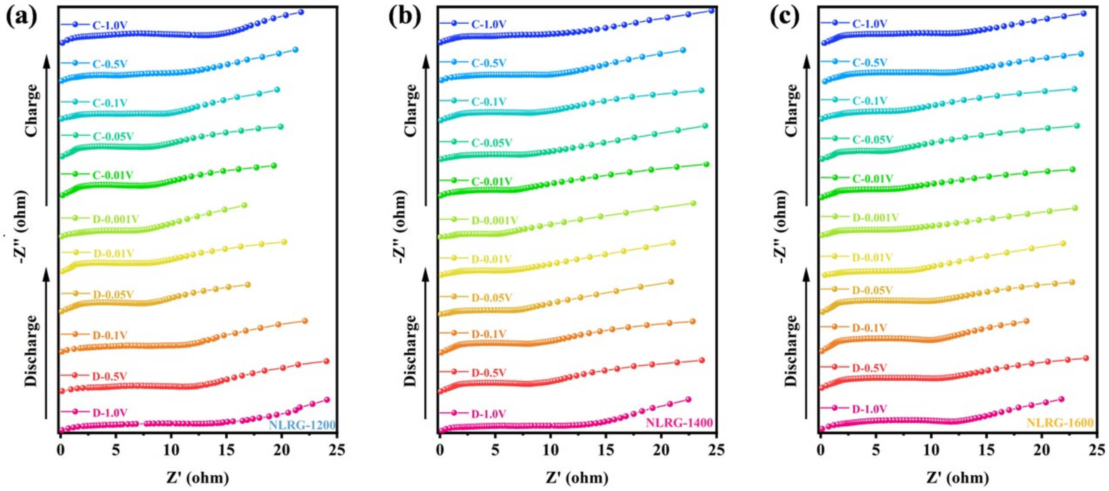

Fig. S6 In-situ EIS Nyquist plots of (a) NLRG-1200, (b) NLRG-1400 and (c) NLRG-1600 during the first discharge/charge cycle.

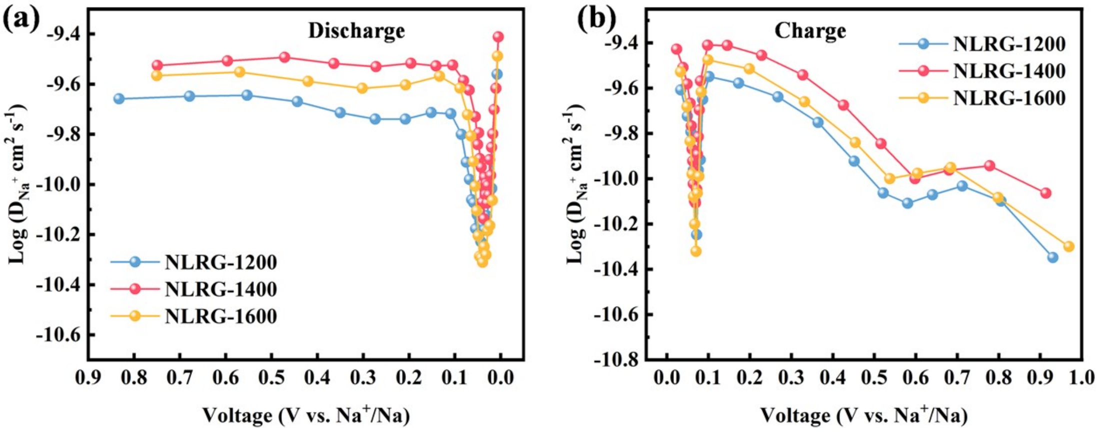

Fig. S7 (a) Sodium-ion diffusion coefficients (D_{Na^+}) as a function of potential during discharge; (b) Sodium-ion diffusion coefficients (D_{Na^+}) as a function of potential during charge.

Table. S6 Comparison of full-cell performance of NLRG-1400 with recently reported hard-carbon-based sodium-ion full cells.

Reference	Cathode material (type)	Hard carbon	Full-cell energy density (based on total active mass of anode + cathode)	Average operating voltage	Initial Reversible Capacity (test condition)	Cycling performance (retention / cycles)
This work	**O3-$NaNi_{1/3}Fe_{1/3}Mn_{1/3}O_2$ [layered oxide]**	**NLRG-1400**	**241 Wh kg^{-1}**	**2.8 V**	**125.8 mAh g^{-1} (based on cathode mass)**	**70.3% / 310 cycles**
28	O3-$NaNi_{1/3}Fe_{1/3}Mn_{1/3}O_2$ [layered oxide]	RG-1300	239 Wh kg^{-1}	3.1 V	283 mAh g^{-1} (based on anode mass)	—
24	O3-$Na_{0.9}[Cu_{0.22}Fe_{0.30}Mn_{0.48}]O_2$ [layered oxide]	PPAC111400	195 Wh kg^{-1}	3.2 V	240 mAh g^{-1} (based on anode mass)	91% / 100 cycles
16	$Na_3V_2(PO_4)_2F_3$ (NVPOF) [polyanionic /	C-HC	239 Wh kg^{-1}	— (two plateaus: 3.8/3.2 V)	98 mAh g^{-1} (based on cathode	80% / 50 cycles

	fluorophosphate]				mass)	
48	$Na_3V_2(PO_4)_3$ (NVP) [polyanionic / NASICON]	HC1300	245.7 Wh kg^{-1}	3.34 V	246.3 mAh g^{-1} (based on anode mass)	~76% / 70 cycles
49	$Na_3V_2(PO_4)_3$ (NVP) [polyanionic / NASICON]	ZGHC1500	260.4 Wh kg^{-1}	3.28 V	413.7 mAh g^{-1} (based on anode mass)	—
52	$Na_3V_2(PO_4)_3$ (NVP) [polyanionic / NASICON]	STHC-MS	266 Wh kg^{-1}	—	104.5 mAh g^{-1} (based on cathode mass)	91.7% / 250 cycles
44	$Na_3V_2(PO_4)_3$ (NVP) [polyanionic / NASICON]	HCUP-40	223.9 Wh kg^{-1}	3.28 V	~108.8 mAh g^{-1} (based on cathode mass)	97.53% / 50 cycles
33	$Na_3V_2(PO_4)_3$ (NVP) [polyanionic / NASICON]	HC-400/1300	213 Wh kg^{-1}	—	163 mAh g^{-1} (based on anode mass)	73.4% / 100 cycles
18	$Na_3V_2(PO_4)_3$ (NVP) [polyanionic / NASICON]	YHC-1200	220 Wh kg^{-1}	—	272.1 mAh g^{-1} (based on anode mass)	82.3% / 300 cycles

Table. S7 Proportions of various components within the C 1s and O 1s spectra of the NLRG-1400 electrode discharged to states of 1.5 V, 1.0 V, 0.5 V, and 0.1 V.

Sample	1.5 V (%)	1.0 V (%)	0.5 V (%)	0.1 V (%)
sp^2 C	73.13	93.44	99.14	99.57
sp^3 C	26.87	6.56	0.86	0.43
C=O	91.40	82.38	60.00	10.90

C-O	8.60	17.62	40.00	89.10

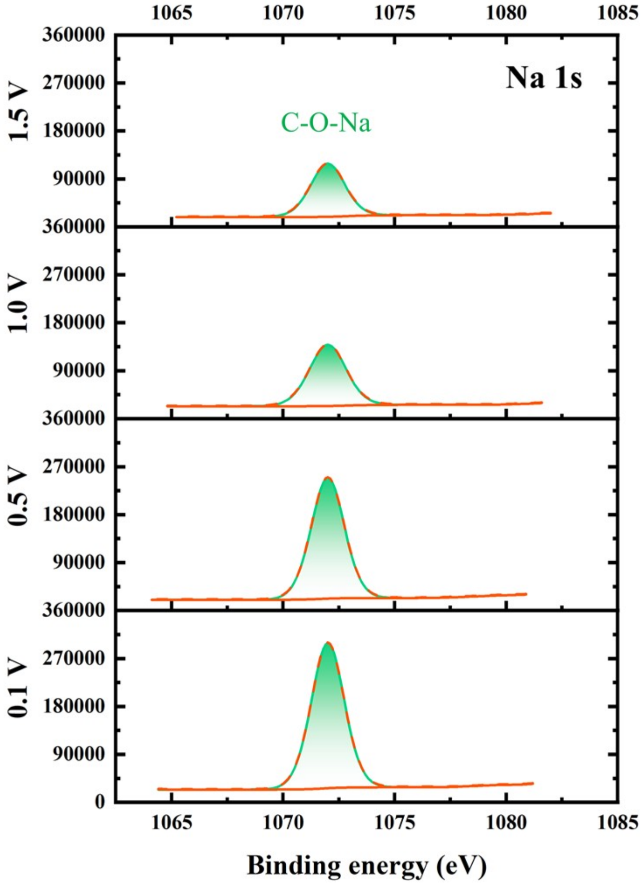

Fig. S8 Ex-situ X-ray photoelectron spectroscopy (XPS) Na 1s spectra of the NLRG-1400 electrode discharged to states of 1.5 V, 1.0 V, 0.5 V, and 0.1 V.

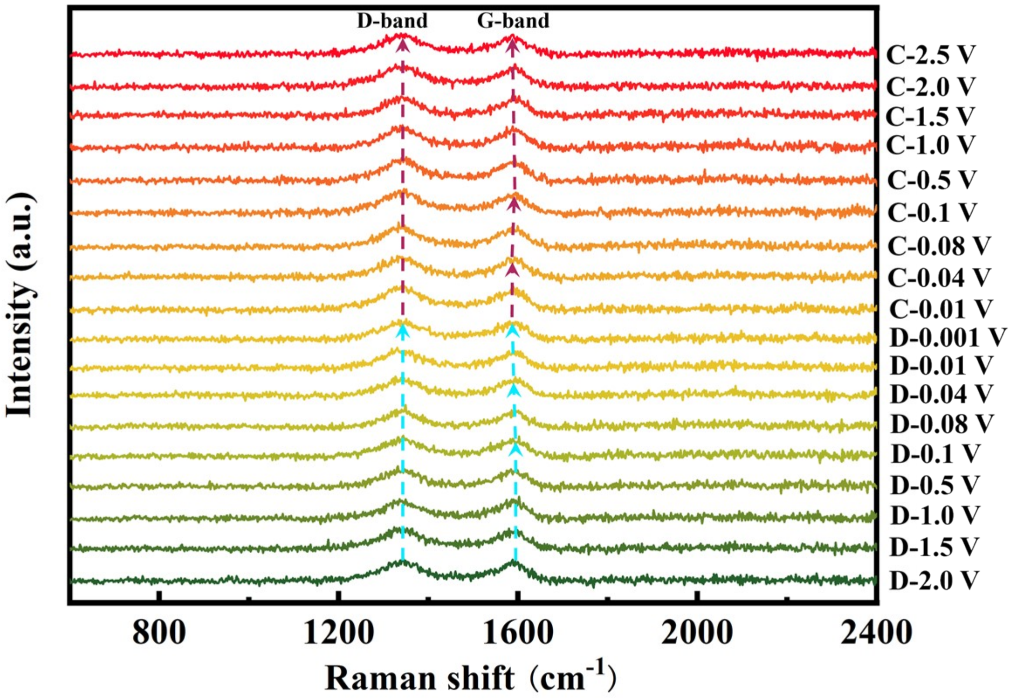

Fig. S9 In-situ Raman spectra of the NLRG-1400 electrode during charge/discharge cycling.

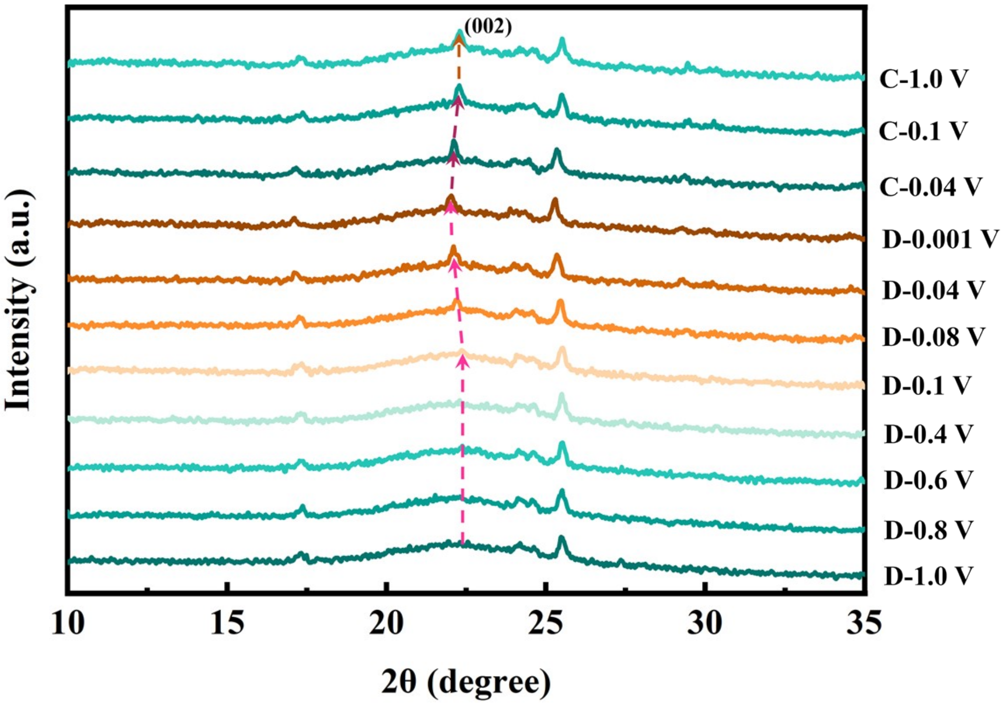

Fig. S10 In-situ XRD patterns of the NLRG-1400 electrode during charge/discharge cycling.

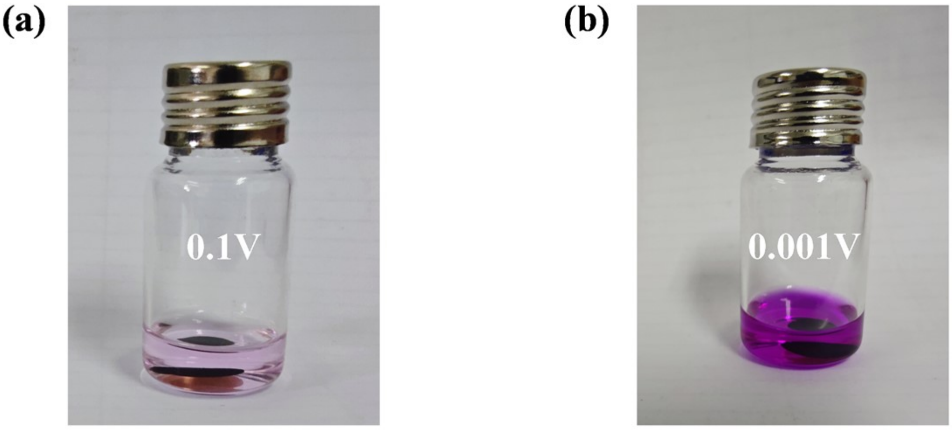

Fig. S11 (a) Photograph of the phenolphthalein–ethanol coloration test for an electrode that had been cycled three times to form a stable SEI film and then discharged to 0.1 V; (b) Photograph of the phenolphthalein–ethanol coloration test for an electrode that had been cycled three times and fully discharged to 0.001 V, after being soaked in dimethyl carbonate (DMC) to partially remove the surface SEI.

References

1. D. Li, X. He, L. Wang, Y. Zhang, X. Wu, M. Ding, C. Gao, Y. Gao and C. Jia, *Chem. Eng. J.* , 2025, **522**, 167350.
2. M. Li, Y. Wang, Y. Zhang and N. Zhang, *Chem. Eng. J.* , 2025, **506**, 160083.
3. D. Li, X. He, L. Wang, M. Ding, C. Gao and C. Jia, *Green Chem.* , 2025, **27**, 14944–14953.
4. L. Zhang, J. Liu, Y. Zhai, S. Zhang, W. Wang, G. Li, L. Sun, H. Li, S. Qi, S. Chen, R. Wang, Q. Ma, J. Just and C. Zhang, *Adv. Mater.*, 2024, **36**, 2313835.
5. M. Ma, K. Yao, X. Zhai, Y. Zhu, X. Yang, D. Fattakhova-Rohlfing, H. K. Liu, S. X. Dou, S. Chong and W. Huang, *Angew. Chem. Int. Ed.*, 2025, **64**, e202513581.
6. M. Ma, K. Yao, Y. Zhu, X. Zhai, S. Qiao, M. Finsterbusch, D. Fattakhova-Rohlfing, H. K. Liu, S. X. Dou, W. Huang and S. Chong, *Angew. Chem. Int. Ed.*, 2026, **65**, e6193851.
7. H. Qi, Y. Du, J. Ding, L. Song, J. Liao, C. Yu, Z. Yuan, S. Chen and X. Zhou, *Nat. Commun.*, 2026, **4631**.
8. Z. Li, Y. Di, Z. Wang, D. Zhang, H. Sun, Q. Sun, Q. Wang, F. Yuan, R. Li and B. Wang, *Green Chem.* , 2025, **28**, 1037–1045.
9. A. Zhao, Y. Fang, X. Ai, H. Yang and Y. Cao, *J. Energy Chem.* , 2021, **60**, 635–

648.

10. S. Chong, B. Lv, S. Qiao, K. Yao, L. Yuan, Z. Liu, H. K. Liu, S. X. Dou and W. Huang, *Angew. Chem. Int. Ed.* , 2025, **64**, e202512894.
11. C. Yuan, Q. Wu, Q. Li, Q. Duan, Y. Li and H. Wang, *ACS Sustainable Chem. Eng.*, 2018, **6**, 8392.
12. F. Luo, C. Yi, D. Yang, D. Fan, W. Liu, X. Qiu and W. Zhang, *Green Chem.*, 2025, **27**, 1703-1713.
13. M. Ma, K. Yao, Y. Wang, D. Fattakhova-Rohlfing and S. Chong, *Adv. Funct. Mater.* , 2024, **34**, 2315662.
14. Z. Wang, S. Qiao, M. Ma, T. Li, H. K. Liu, S. X. Dou and S. Chong, *ACS Nano* , 2025, **19**, 15148–15160.
15. B. Chen, L. Zhong, M. Lu, W. Jian, S. Sun, Q. Meng, T. Wang, W. Zhang and X. Qiu, *Green Chem.* , 2024, **26**, 7919–7930.
16. D. Sun, B. Luo, H. Wang, Y. Tang, X. Ji and L. Wang, *Nano Energy* , 2019, **64**, 103937.
17. Y. Chen, H. Sun, X.-X. He, Q. Chen, J.-H. Zhao, Y. Wei, X. Wu, Z. Zhang, Y. Jiang and S.-L. Chou, *Small* , 2024, **20**, 2307132.
18. J. Duan, P. Yang, Z. Xu, H. Hu, Z. Zhang, M. Bai, G. Zeng and Z. Chen, *Chem. Eng. J.* , 2025, **508**, 161184.
19. L. K. Iglesias, S. D. Marks, N. Rampal, E. N. Antonio, R. F. de Menezes, L. Zhang, D. Olds, S. E. Weitzner, K. G. Sprenger, L. F. Wan and M. F. Toney, *Small* , 2025, **21**, 2505561.
20. Q. Jiang, Z. Zhang, S. Yin, Z. Guo, S. Wang and C. Feng, Appl. Surf. Sci. , 2016, **379**, 73–82.
21. C. d. M. S. Rios, V. Simone, L. Simonin, S. Martinet and C. Dupont, *Biomass Bioenergy* , 2018, **117**, 32–37.
22. C. Bommier, W. Luo, W.-Y. Gao, A. Greaney, S. Ma and X. Ji, *Carbon*, 2014, **76**, 165.
23. B. M. Upton and A. M. Kasko, *Chem. Rev.*, 2016, **116**, 2275.
24. Y. Li, L. Mu, Y.-S. Hu, H. Li, L. Chen and X. Huang, *Energy Storage Mater.*,

2016, **2**, 139.

25. H. Liu, M. Jia, N. Sun, B. Cao, R. Chen, Q. Zhu, F. Wu, N. Qiao and B. Xu, *ACS Appl. Mater. Interfaces*, 2015, **7**, 27124.
26. Y. Hu, B. Li, X. Jiao, C. Zhang, X. Dai and J. Song, *Adv. Funct. Mater.*, 2018, **28**, 1801010.
27. Y. Bai, Z. Wang, C. Wu, R. Xu, F. Wu, Y. Liu, H. Li, Y. Li, J. Lu and K. Amine, *ACS Appl. Mater. Interfaces*, 2015, **7**, 5598.
28. J. Wang, W. Lv, Q. Ren, L. Yan, L. Zhang and Z. Shi, *Appl. Surf. Sci.*, 2021, **558**, 149824.
29. X. Zhang, Z. Hou, M. Jiang, J. Peng, H. Ma, Y. Gao and J.-G. Wang, *Small*, 2024, **20**, 2311778.
30. G. Zhang, L. Zhang, Q. Ren, L. Yan, F. Zhang, W. Lv and Z. Shi, *ACS Appl. Mater. Interfaces*, 2021, **13**, 31650.
31. X. Li, J. Zhang, R. Yuan, B. Zhao, C. Qiu, D. Wang, M. Yuan, A. Li, H. Liu, X. Chen and H. Song, *Chem. Eng. J.*, 2025, **520**, 166187.
32. X. Li, J. Zhang, J. Zhang, L. Guo, H. Zhang, R. Yuan, H. Liu, A. Li, X. Chen and H. Song, *ACS Nano*, 2025, **19**, 14829.
33. B. Wang, S. Zhang, X. Jia, F. Yuan, H. Sun, Z. Li, Q. Sun, Q. Wang and D. Zhang, *Chem. Eng. J.*, 2024, **499**, 156126.
34. X. Huang, H. Wu, X. Wu, W. Su and P. Li, *Pharmacol. Res.*, 2025, **219**, 107871.
35. A. Wang, G. Zhang, M. Li, Y. Sun, Y. Tang, K. Sun, J.-M. Lee, G. Fu and J. Jiang, *Prog. Mater. Sci.*, 2025, **152**, 101452.
36. C. M. Ghimbeu, B. Zhang, A. Martinez de Yuso, B. Rety and J.-M. Tarascon, *Carbon*, 2019, **153**, 634.
37. N. K. Dayarathne, C. Shi, X. Song, C. Yan, D. Wang, H. Wang, Y. L. Zhong and Z. Zhang, *Energy Storage Mater.*, 2025, **83**, 104705.
38. A. T. P. Hoang and K.-W. Kim, *J. Environ. Chem. Eng.*, 2025, **13**, 116236.
39. W. Sun, H. Shen and J. Cao, *Mater. Des.*, 2016, **96**, 392.
40. A. Beda, P.-L. Taberna, P. Simon and C. M. Ghimbeu, *Carbon*, 2018, **139**, 248.
41. C. Fan, R. Zhang, X. Luo, Z. Hu, W. Zhou, W. Zhang, J. Liu and J. Liu, *Carbon*,

2023, **205**, 353.

42. R. Xie, M. Huang, C. Feng, Z. Shao, X. Cheng and F. Han, *ACS Appl. Energy Mater.*, 2025, **8**, 17404–17415.
43. Z. Tang, R. Zhang, H. Wang, S. Zhou, Z. Pan, Y. Huang, D. Sun, Y. Tang, X. Ji, K. Amine and M. Shao, *Nat. Commun.*, 2023, **14**, 6024.
44. Y. Liu, S. Dai, J. Deng, D. Jiang, X. Ji, Q. Meng, H. Wang and L. Liu, *J. Colloid Interface Sci.*, 2025, **686**, 136.
45. Y. Aniskevich, J. H. Yu, J.-Y. Kim, S. Komaba and S.-T. Myung, *Adv. Energy Mater.*, 2024, **14**, 2304300.
46. Q. Hu, L. Xu, G. Liu, J. Hu, X. Ji and Y. Wu, *ACS Nano*, 2024, **18**, 21491.
47. W. Li, J. Li, B. W. Biney, Y. Yan, X. Lu, H. Li, H. Liu, W. Xia, D. Liu, K. Chen and A. Guo, *Energy Storage Mater.*, 2025, **74**, 103867.
48. X. Zhang, Y. Cao, G. Li, G. Liu, X. Dong, Y. Wang, X. Jiang, X. Zhang and Y. Xia, *Small*, 2024, **20**, 2311197.
49. C. Qiu, A. Li, D. Qiu, Y. Wu, Z. Jiang, J. Zhang, J. Xiao, R. Yuan, Z. Jiang, X. Liu, X. Chen and H. Song, *ACS Nano*, 2024, **18**, 11941.
50. Y. Wang, Z. Yi, L. Xie, Y. Mao, W. Ji, Z. Liu, X. Wei, F. Su and C.-M. Chen, *Adv. Mater.*, 2024, **36**, 2401249.
51. J.-L. Xia, D. Yan, L.-P. Guo, X.-L. Dong, W.-C. Li and A.-H. Lu, *Adv. Mater.*, 2020, **32**, 2000447.
52. Z. Wen, R. Zhao, T. Tian, T. Zhang, X. Wang, X. Yang, W. Song, Y. Chen, J. Ding and W. Hu, *Adv. Mater.*, 2025, **37**, 2420251.
53. X. Liu, M. Zhang, X. Wang, Y. Peng, Y. Liu, S. Ullah, Z. Duan, W. Gao, B. Song, M. Wei, J. He, Z. Li and Y. Wu, *Adv. Mater.*, 2025, **37**, 2410673.
54. Z. Wang, X. Feng, Y. Bai, H. Yang, R. Dong, X. Wang, H. Xu, Q. Wang, H. Li, H. Gao and C. Wu, *Adv. Energy Mater.*, 2021, **11**, 2003854.